

Journal of Biomedical Optics

BiomedicalOptics.SPIEDigitalLibrary.org

Radiotherapy fiber dosimeter probes based on silver-only coated hollow glass waveguides

Arash Darafsheh
Jeffrey E. Melzer
James A. Harrington
Alireza Kassaei
Jarod C. Finlay

SPIE.

Arash Darafsheh, Jeffrey E. Melzer, James A. Harrington, Alireza Kassaei, Jarod C. Finlay, "Radiotherapy fiber dosimeter probes based on silver-only coated hollow glass waveguides," *J. Biomed. Opt.* 23(1), 015006 (2018), doi: 10.1117/1.JBO.23.1.015006.

Radiotherapy fiber dosimeter probes based on silver-only coated hollow glass waveguides

Arash Darafsheh,^{a,*} Jeffrey E. Melzer,^b James A. Harrington,^b Alireza Kassaei,^c and Jarod C. Finlay^c

^aWashington University School of Medicine, Department of Radiation Oncology, St. Louis, Missouri, United States

^bRutgers University, Department of Material Science and Engineering, Piscataway, New Jersey, United States

^cUniversity of Pennsylvania, Department of Radiation Oncology, Philadelphia, Pennsylvania, United States

Abstract. Manifestation of Čerenkov radiation as a contaminating signal is a significant issue in radiation therapy dose measurement by fiber-coupled scintillator dosimeters. To enhance the scintillation signal transmission while minimizing Čerenkov radiation contamination, we designed a fiber probe using a silver-only coated hollow waveguide (HWG). The HWG with scintillator inserted in its tip, embedded in tissue-mimicking phantoms, was irradiated with clinical electron and photon beams generated by a medical linear accelerator. Optical spectra of the irradiated tip were taken using a fiber spectrometer, and the signal was deconvolved with a linear fitting algorithm. The resultant decomposed spectra of the scintillator with and without Čerenkov correction were in agreement with measurements performed by a standard electron diode and ion chamber for electron and photon beam dosimetry, respectively, indicating the minimal effect of Čerenkov contamination in the HWG-based dosimeter. Furthermore, compared with a silver/dielectric-coated HWG fiber dosimeter design, we observed higher signal transmission in the design based on the use of silver-only HWG. © 2018 Society of Photo-Optical Instrumentation Engineers (SPIE) [DOI: 10.1117/1.JBO.23.1.015006]

Keywords: radiation therapy; dosimetry; hollow waveguide; optical fiber; Čerenkov radiation; spectroscopy.

Paper 170587PR received Sep. 6, 2017; accepted for publication Dec. 21, 2017; published online Jan. 16, 2018.

1 Introduction

Accurate measurement of the absorbed dose, i.e., energy deposited by the ionizing radiation in tissue, is an important part of radiation therapy quality assurance. In the context of radiotherapy dosimetry, fiber optic dosimeters^{1–20} have drawn great attention because they show unique practical advantageous properties including the ability to perform *in vivo*, real-time, and intracavity measurements with high spatial resolution due to their small physical size. These features make them ideal candidates for many applications in radiation therapy dosimetry, such as in high-dose-rate brachytherapy, intensity-modulated radiation therapy, superficial therapy, stereotactic radiosurgery, proton therapy, and small-field dosimetry.²¹

In a typical fiber optic dosimeter system, interaction of the ionizing radiation with the scintillator generates an optical signal proportional to the absorbed dose in the irradiated scintillator, which is collected and transmitted by the optical fiber to a detector. However, a significant problem with fiber optic dosimetry is that the signal received by the detector through the fiber is contaminated with Čerenkov radiation, which may not be directly proportional to the dose.^{22,23} When optical fibers pass through ionizing radiation fields of high energy, Čerenkov radiation generated inside the fiber core is guided through the fiber if the emitted photon hits the core-cladding boundary with an angle greater than the critical angle for total internal reflection. Transmission of Čerenkov radiation is, therefore, dependent on the angle between the particle track and the fiber axis. Therefore, the total signal must be corrected for the contribution of

Čerenkov radiation in order to accurately measure the absorbed dose in the scintillator.

Some efforts have been devoted to developing methods to minimize the influence of Čerenkov radiation contamination in order to improve the accuracy of fiber optic dosimetry. These methods include the (i) Subtraction method^{22,24} based on using a parallel bare fiber identical to the one that is connected to the scintillator piece to produce similar Čerenkov light that can be subtracted from the total signal. However, this technique is not reliable for radiation fields with high-dose gradient. (ii) Optical filtering²⁵ where a long-wavelength-emitting scintillator in conjunction with a long pass filter is used to selectively measure the signal in longer wavelengths of the spectrum where the intensity of the Čerenkov radiation is weaker due to its λ^{-3} intensity profile. However, this method is not very effective since the filtered signal is still contaminated with Čerenkov radiation due to the fact that the Čerenkov radiation has a continuous spectrum. (iii) Temporal separation²⁶ that relies on different time scales associated with Čerenkov emission and scintillation processes. This method requires fast responding electronics and works only with pulsed radiation fields. (iv) Chromatic removal^{27–29} that requires two different optical filters to measure the signal at two different spectral regions; the dose is then calculated by using coefficients obtained from calibration. (v) Rigorous spectral separation based on acquiring the whole spectrum of the transmitted signal and decomposing it into its constituting components using *a priori* knowledge of the spectral shape of the scintillation signal and Čerenkov radiation.⁹

The development of waveguides with hollow cores was a milestone in infrared light transmission,^{30,31} where conventional

*Address all correspondence to: Arash Darafsheh, E-mail: arash.darafsheh@wustl.edu

solid-core fibers dramatically suffer from optical power loss. Hollow waveguides (HWG) structurally are composed of a glass or plastic capillary coated internally with a metal/dielectric layer to enhance the infrared transmission in the waveguide. In the context of fiber optic dosimetry, it has been suggested³² that the use of HWG with air core instead of conventional solid-core fibers would reduce the deteriorating effect of Čerenkov radiation due to the fact that the production of Čerenkov light is minimal in air since its refractive index is very close to 1; such HWGs, however, conventionally have optimal design parameters for transmission of infrared wavelengths,^{31,33} whereas the scintillators of interest in fiber optic dosimeters emit primarily visible light.

In this work, in order to enhance the transmission of the scintillation signal while minimizing Čerenkov radiation contamination, we designed and evaluated the performance of an HWG-based dosimeter system using silver-only coated (i.e., without the additional dielectric coating) HWG. The silver-only coated HWG³⁴ has been designed to have superior transmission in visible range of the spectrum compared with the conventional HWGs with silver/dielectric coating that are optimized for transmission of infrared light. In order to evaluate the performance of our dosimeter, optical spectra of the irradiated dosimeter tip with therapeutic electron and photon beams were taken using a fiber spectrometer, and the signal was deconvolved with a linear fitting algorithm. The resultant decomposed spectra of the scintillator with and without Čerenkov correction were in agreement with measurements performed by standard electron diode and ion chamber for electron and photon beam dosimetry, respectively, indicating the minimal effect of Čerenkov contamination. Compared with a silver/dielectric-coated HWG fiber dosimeter design, we observed higher signal transmission in the design based on the use of silver-only coated HWG.

2 Čerenkov Radiation

Čerenkov radiation has attracted a considerable amount of recent research interest for its potential applications in life sciences and engineering, such as in molecular imaging,^{35–48} particle detection,^{49–53} ionizing radiation quality assurance, and beam monitoring.^{54–58}

Čerenkov radiation is a visible light emitted from a dielectric medium when charged particles with velocities greater than the phase velocity of the light in that medium, i.e., $v > c/n$, pass through it. The passage of the charged particles induces dipole oscillations through polarization of the medium whose relaxation lead to emission of light when $v > c/n$ due to the constructive interference of the emitted waves. Čerenkov radiation is a polarized, coherent, and directional emission; its direction is along the surface of a cone that makes the half-angle $\theta = \cos^{-1}(n\beta)^{-1}$ with the particle track, where n is the refractive index of the medium and $\beta = v/c$ is the ratio of the velocity of the particle to that of light.

To induce Čerenkov radiation, a charged particle must satisfy the $v > c/n$ condition; the minimum energy required is given as

$$E_{\min} = m_0 c^2 \left(\frac{1}{\sqrt{1 - n^{-2}}} - 1 \right), \quad (1)$$

where m_0 is the rest mass of the particle. The threshold electron energies to generate Čerenkov radiation in water ($n = 1.33$) and pure silica ($n = 1.55$) are $E_{\min} = 264$ and 158 keV, respectively. These energies are far below the energies of megavoltage beams

used in modern radiotherapy. The passage of these high energy primary and secondary electrons through the fiber optic dosimeters generates Čerenkov light that is the dominant source of the unwanted background signal in the output signal.

The number of Čerenkov photons generated by a charged particle with charge ze , where e is the charge of an electron, along path length l in the wavelength region between λ_1 and λ_2 ($\lambda_1 < \lambda_2$) is proportional to λ^{-2} and is given as

$$N = 2\pi\alpha z^2 l (\lambda_1^{-1} - \lambda_2^{-1}) [1 - (n\beta)^{-2}], \quad (2)$$

where $\alpha = e^2/(4\pi\epsilon_0\hbar c) \approx 1/137$ is the fine structure constant.⁵⁹

The amount of Čerenkov light contamination recorded by the optical fiber dosimeter depends on the angular configuration and spatial position and therefore is not constant so straightforward subtraction as a calibration constant cannot be done. However, the spectral characteristic of the Čerenkov radiation can be used to decompose the output signal through rigorous spectroscopy. Specifically, Čerenkov radiation has a continuous spectrum spanning from near-ultraviolet to near-infrared, restricted from both ends of the visible spectrum by the absorption spectrum of the material in which it is generated, with light intensity decreasing proportional to λ^{-3} as the wavelength increases.

3 Materials and Methods

We designed and fabricated a fiber optic dosimeter probe with the following main components:

- i. a plastic scintillator tip to convert the radiation absorbed dose to an optical signal,
- ii. a silver-only coated glass HWG to transmit the scintillation signal to an optical fiber,
- iii. a solid-core optical fiber to transmit the signal from the HWG to the spectrometer,
- iv. a spectrometer to acquire the spectrum of light collected by the HWG and transmitted by the fiber, and
- v. a computer for signal processing to calculate the radiation dose.

A schematic illustration of the dosimeter design is shown in Figs. 1(a) and 1(b). A 5-mm length piece of BCF-12 (Saint-Gobain Crystals) plastic scintillating fiber with ~ 1 mm diameter was inserted at the tip of a silver-only coated glass HWG with 50 cm length and ~ 1 mm inner and 1.2 mm outer diameters. A 15-m-long silica optical fiber (FT400UMT, Thorlabs) with numerical aperture $NA = 0.39$ (core refractive index 1.51 and cladding index 1.46 at 500 nm) and core diameter of 400 μm was inserted 1 cm into the HWG from the other end to capture and transport the emitted light from the scintillator to the spectrometer. In order to compare the operation of different types of HWG-based dosimeters, we made another dosimeter based on a silver/dielectric-coating HWG (Polymicro Technologies) with 20 cm length and 1 mm ID, in which we inserted the same scintillator piece.

It should be mentioned that the choice of 1 mm as the inner diameter of the HWGs used in our work was to provide maximizing throughput while not sacrificing too much in the way of robustness, as there is a tradeoff between robustness and throughput. Since the power loss in a HWG is inversely proportional to the cube of the bore radius,³⁰ increasing the bore

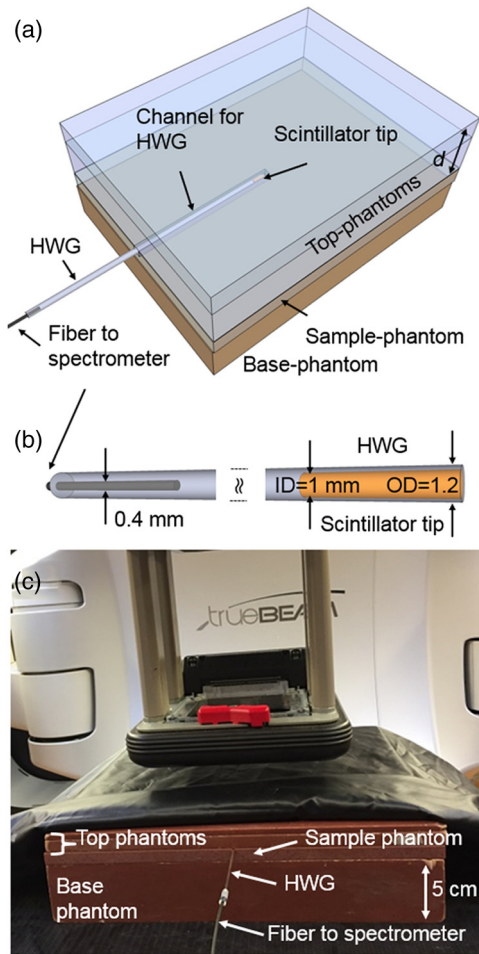


Fig. 1 (a) Schematic of the experimental setup with the fiber dosimeter composed of plastic scintillator inserted in an HWG coupled with a solid-core optical fiber. (b) Expanded view of the probe. (c) Picture of the experimental setup with a TrueBeam™ clinical linear accelerator: the fiber probe was positioned in a virtual water phantom labeled as the sample-phantom and additional phantom layers (top phantoms) were placed over the sample phantom sequentially.

diameter reduces the transmission loss. However, practically as the waveguide bore size is increases, we reach a point at which we have a rigid glass rod instead of a relatively flexible HWG. In practice, the largest hollow glass waveguide size that is typically used is ~ 1 mm inner diameter.

Optical spectroscopy was performed by a thermoelectrically cooled CCD array spectrometer (BTC112E, BWTEK Inc.) with 0.4-nm spectral resolution. In order to minimize potential direct interaction of ionizing radiation with its CCD, the spectrometer was placed outside the treatment room. Dark current spectra were acquired with the spectrometer's input aperture covered and were subtracted from each spectrum acquired. The spectra were corrected for wavelength-dependent instrument response and wavelength-dependent transmission of fibers using an instrument-specific calibration function. This function was determined by taking the ratio of the measured spectrum of a lamp with a NIST-traceable calibration (LS1-cal, Ocean Optics) to its known spectrum.

The fiber probe, placed in a $30 \times 30 \times 1$ cm³ virtual water phantom (Standard Imaging), was irradiated by 6-MeV energy electron beam and 6- and 15-MV photon beams in a square field size of 10×10 cm² generated using a clinical medical linear

accelerator (TrueBeam™, Varian Medical Systems), see Fig. 1(c). The selected electron beam energy is much greater than the energy threshold required for emission of Čerenkov radiation in pure silica ($E_{\min} \approx 0.158$ MeV). In the case of irradiation with 6- and 15-MV photons, the secondary liberated electrons would have energies much higher than the threshold energy needed to generate Čerenkov radiation, as we have previously observed Čerenkov emission from radiation at these photon energies in silica fibers.¹⁵ The HWG was completely embedded in the sample-phantom that provides a way to place additional phantom layers on top of the sample-phantom. Additional phantom layers were sequentially added after each measurement to provide measurements at different phantom depths. The distance from the source to the top surface of the top most phantom (SSD) was adjusted to 100 and 90 cm for the electron beam and photon beam irradiation, respectively.

In each case, the recorded spectrum, corrected for instrument response, was analyzed as a linear combination of basis luminescence spectra using a singular value decomposition (SVD) fitting algorithm implemented in MATLAB®. We considered the recorded optical signal (S_{tot}) by the spectrometer as the linear superposition of two basis components: plastic scintillation (S_{sc}) and the Čerenkov radiation (\check{C}_f) generated in the fiber scintillator. The basis spectrum for the Čerenkov radiation is calculated from the theoretical λ^{-3} dependency expected for Čerenkov radiation, where λ is the wavelength of light. We experimentally verified the λ^{-3} dependency by curve fitting to spectra obtained from irradiated standalone fibers in various conditions. The basis spectrum for the plastic scintillator was obtained according to the following manner. First, we recorded the spectrum of the irradiated fiber probe with its scintillator tip connected. Then, we detached the scintillator tip from the HWG and recorded the spectrum of the irradiated bare HWG. By subtracting the latter from the former, we obtained the basis spectrum for the scintillator. We verified that basis spectrum by irradiating the scintillator with incident beams of energies below the threshold for generating Čerenkov radiation. The SVD fitting algorithm has additional Fourier terms to take into account potential presence of any other contributions. The two basis spectra and the Fourier series are fit to the instrument-corrected data using

$$S_{\text{tot}} = a_{100}S_{\text{sc}} + b_{100}\check{C}_f + c_{1.4}F_0, \quad (3)$$

where the numbers in subscript are the weights used in the SVD fitting algorithm. This choice of the weighting factors provided reliable fits to the experimental data. It should be noted that their exact values are not critical as the SVD fits were remarkably insensitive to the choice of weighting factors.

4 Results and Discussion

The normalized basis spectra for the Čerenkov and scintillator radiation used in the SVD fitting algorithm are presented in Fig. 2. Čerenkov light has a continuous spectrum with λ^{-3} wavelength dependency and the BCF-12 scintillator has a broad emission spectrum with a peak at $\lambda \sim 435$ nm.

A series of spectra collected at various depths in solid water phantom irradiated with 6-MeV electron beam and 6- and 15-MV photon beams is presented in Figs. 3(a)–3(c), respectively. For 6-MeV electron beam irradiation, the measurements were performed at depths of 5 to 30 mm corresponding to the practical range of electrons in the phantom. For 6- and 15-MV

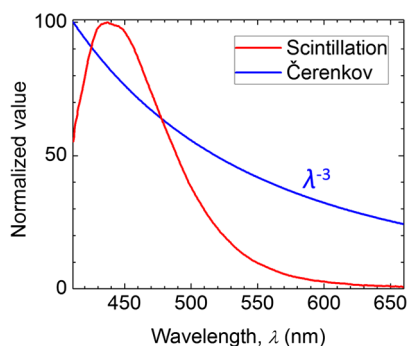


Fig. 2 Basis spectra for the Čerenkov radiation and BCF-12 scintillator with peak emission at $\lambda \sim 435$ used for SVD method. Spectra were normalized to 100 within the data treatment spectral range of $\lambda = 410$ to 660 nm.

photon irradiation, the measurements were performed at phantom depths of 5 to 125 mm. We assumed that the measured spectrum in each condition is a superposition of the BCF-12 scintillation on an extremely weak continuous Čerenkov radiation background generated in the scintillator. By using the SVD algorithm, we decomposed the recorded signal into its constituting components and the coefficients a_{100} defined in Eq. (3) for each beam and depth condition were used as the measure of the absorbed dose. Figure 3(d) shows a typical spectrum obtained at 1.5 cm phantom depth, irradiated with a 6-MV photon beam, with the corresponding components from the SVD fit, showing less than two orders of magnitude in intensity of the Čerenkov contamination.

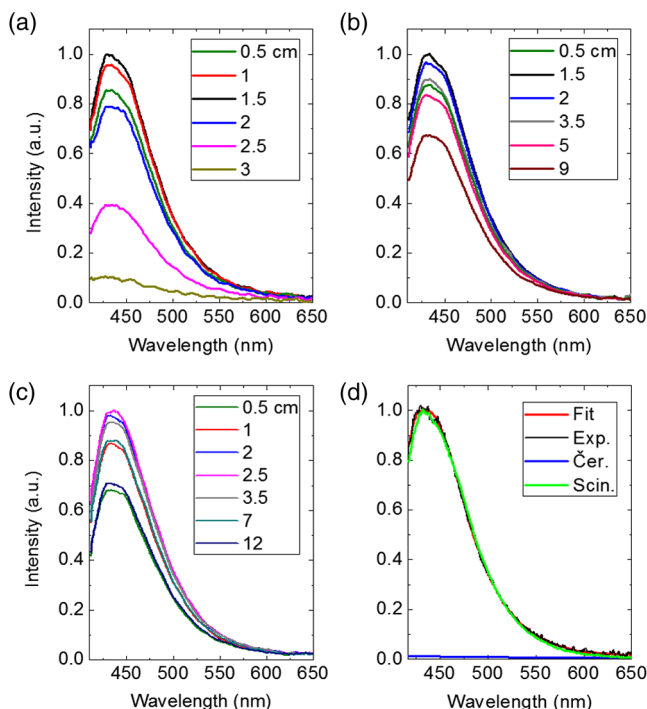


Fig. 3 Series of recorded spectra at different phantom depths obtained from the Ag-only coated HWG-based fiber dosimeter irradiated by (a) 6-MeV electron beam, (b) 6-MV photon beam, and (c) 15-MV photon beam with 10×10 cm² field size. (d) Spectrum obtained at 1.5 cm phantom depth, irradiated with a 6-MV photon beam, with the corresponding components from the SVD fit showing negligible Čerenkov contamination. All spectra were normalized to 1.

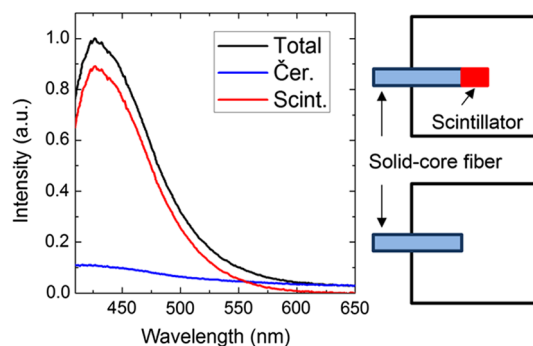


Fig. 4 Black curve is the spectrum of the scintillator directly connected to a solid-core fiber placed at the center of a 10×10 cm² photon field with 6-MV energy (corresponding to the geometry shown in the top inset). Blue graph is the spectrum of the fiber with scintillator piece removed (corresponding to the bottom inset). Red graph is the subtraction of the Čerenkov spectrum from the total signal.

Figure 4 shows the spectrum of a scintillator piece directly connected to the solid-core fiber (i.e., HWG was not used) irradiated with a 6-MV photon beam with 10×10 cm² field size. The scintillator tip was placed at the center of the field, as schematically shown in the inset. The spectrum obtained from the fiber with scintillator removed, which shows only Čerenkov radiation is also plotted in Fig. 4. It can be seen that the contribution of the Čerenkov radiation in the output signal peak intensity is $\sim 10\%$, and integrating the signal shows that $\sim 20\%$ of the total optical power is due to Čerenkov radiation. This comparison shows that the use of HWGs significantly minimizes the contribution of the Čerenkov radiation in the output signal.

The measured absorbed dose as a function of depth in phantom for the 6-MeV electron beam and for the 6- and 15-MV photon beams are presented in Figs. 5(a)–5(c), respectively. The hollow circles correspond to the a_{100} coefficients calculated with considering the Čerenkov basis spectrum, whereas the solid circles correspond to the fit without considering the Čerenkov basis spectrum. The solid lines in Fig. 5 are the depth dose profiles measured by a standard diode-based and ion chamber-based radiation detectors designed for measurements in clinical electron and photon beams, respectively, that were acquired as part of the commissioning procedure for the linear accelerator, in accordance with standard commissioning procedures.⁶⁰ The resultant decomposed spectra of the HWG-based scintillator dosimeter with and without Čerenkov correction are in agreement within 3% with measurements performed by an electron diode for the electron beam and ion chamber for the photon beam, indicating the minimal effect of Čerenkov contamination.

In order to compare the light transmission in the system based on silver-only HWG and a dosimeter system based on a conventional silver/dielectric HWG, in Fig. 6 we present the spectra obtained from both probes irradiated with 6-MV photon beam. It can be seen that the peak signal intensity in the former is more than twice as that in the latter demonstrating superior transmission of visible light in silver-only coated HWG. Also, the total optical power, calculated as the area under each graph, in the former is more than triple as that in the latter. It should be noted that the length of the silver-only HWG is 50 cm whereas the length of the silver-dielectric HWG is 20 cm. Due to the relatively low attenuation coefficient

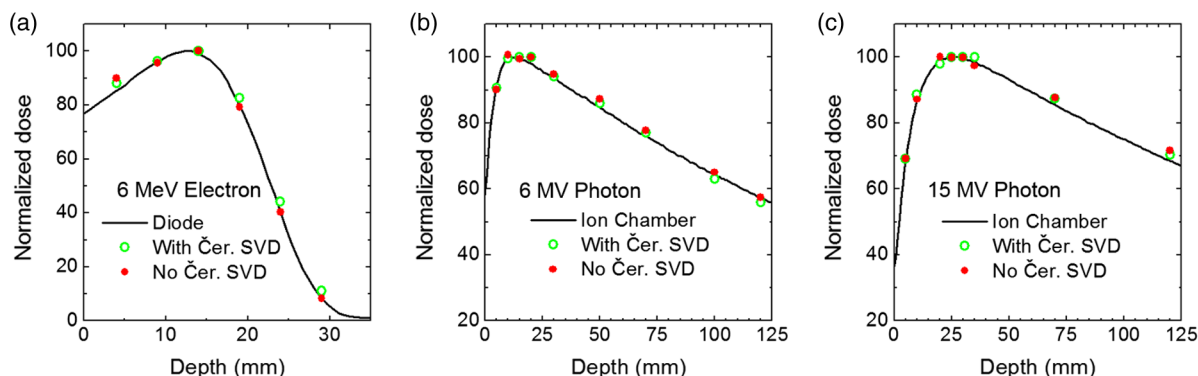


Fig. 5 Dose measurement versus depth in phantom for (a) 6-MeV electron, (b) 6-MV photon beam, and (c) 15-MV photon beam. Solid lines represent measurements performed by an electron diode and ion chamber in (a) and (b), respectively. Solid and hollow circles represent dose measurement using the fiber scintillator without and with Čerenkov correction.

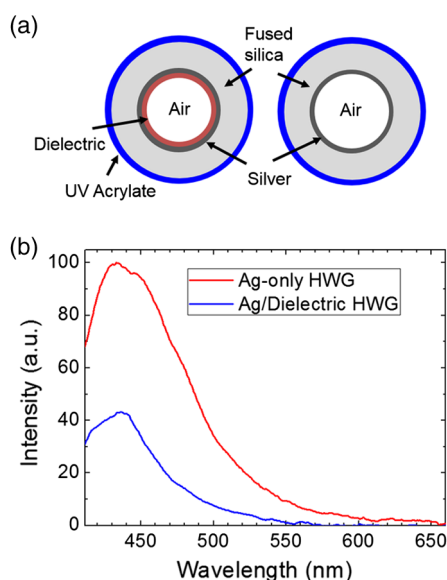


Fig. 6 (a) Schematic cross section of HWGs with silver/dielectric and silver-only coating (drawn not to scale). (b) Comparison between light transmission in a fiber dosimeter system composed of an HWG with silver-only coating (50 cm length) and silver/dielectric coating (20 cm length) irradiated with 6-MV photon beam. The former shows two time higher intensity and three times higher total power transmission compared with the latter.

(~ 0.5 dB/m) in the HWG, we estimate that the output power of an identical 20-cm-length silver-only HWG would be $\sim 3.5\%$ more than that of a 50-cm-length silver-only HWG presented in Fig. 6.

5 Conclusion

Fiber optic probes are interesting tools for radiation therapy quality assurance. In order to enhance the scintillation signal transmission while minimizing the problematic effect of Čerenkov radiation contamination, we designed a fiber optic dosimeter probe using a silver-only coated HWG. We evaluated the dosimeter's performance in ionizing radiation fields of therapeutic electron and photon beams generated by a medical linear accelerator. Optical spectra of the irradiated tip were taken using a fiber spectrometer, and the signal was deconvolved with a

linear fitting algorithm. The resultant decomposed spectra of the scintillator with and without Čerenkov correction were in agreement with measurements performed by an electron diode and ion chamber indicating the minimal effect of Čerenkov radiation contamination. Compared with a silver/dielectric-coated HWG fiber dosimeter design, we observed approximately three times higher signal transmission in the design based on the use of silver-only HWG. This increase in the optical throughput would specifically be more helpful for low SNR scintillation detection scenarios (e.g., near the field edges or deeper depths where the dose is lower).

Compared with all-plastic solid-core fiber dosimeter system, the HWG-based designs using hollow glass waveguides have negligible Čerenkov radiation contamination, but they have higher light attenuation and are more fragile and less flexible. The dosimeter design can be further optimized by improving the optical coupling between the HWG and the solid-core fiber. The mechanical flexibility of the design can be increased by using a hollow plastic polycarbonate waveguides instead of the hollow glass waveguide.

Disclosures

The authors have no relevant financial interests in this article and no potential conflicts of interest to disclose.

References

1. A. Darafsheh et al., "Proton therapy dosimetry using the scintillation of the silica fibers," *Opt. Lett.* **42**(4), 847–850 (2017).
2. L. Beaulieu and S. Beddar, "Review of plastic and liquid scintillation dosimetry for photon, electron, and proton therapy," *Phys. Med. Biol.* **61**(20), R305–R343 (2016).
3. L. Wootton et al., "Real-time in vivo rectal wall dosimetry using plastic scintillation detectors for patients with prostate cancer," *Phys. Med. Biol.* **59**(3), 647–660 (2014).
4. J. C. Gagnon et al., "Dosimetric performance and array assessment of plastic scintillation detectors for stereotactic radiosurgery quality assurance," *Med. Phys.* **39**(1), 429–436 (2012).
5. M. Guillot et al., "A new water-equivalent 2D plastic scintillation detectors array for the dosimetry of megavoltage energy photon beams in radiation therapy," *Med. Phys.* **38**(12), 6763–6774 (2011).
6. F. Theriault-Proulx et al., "A phantom study of an in vivo dosimetry system using plastic scintillation detectors for real-time verification of ^{192}Ir HDR brachytherapy," *Med. Phys.* **38**(5), 2542–2551 (2011).
7. J. Lambert et al., "A plastic scintillation dosimeter for high dose rate brachytherapy," *Phys. Med. Biol.* **51**(21), 5505–5516 (2006).

8. A. Darafsheh et al., "The visible signal responsible for proton therapy dosimetry using bare optical fibers is not Čerenkov radiation," *Med. Phys.* **43**(11), 5973–5980 (2016).
9. A. Darafsheh et al., "Spectroscopic separation of Čerenkov radiation in high-resolution radiation fiber dosimeters," *J. Biomed. Opt.* **20**(9), 095001 (2015).
10. A. Darafsheh et al., "On the origin of the visible light responsible for proton dose measurement using plastic optical fibers," *Proc. SPIE* **10056**, 100560V (2017).
11. A. Darafsheh et al., "Proton therapy dosimetry by using silica glass optical fiber microprobes," *Proc. SPIE* **10058**, 100580B (2017).
12. A. Darafsheh et al., "Fiber optic probes based on silver-only coated hollow glass waveguides for ionizing beam radiation dosimetry," *Proc. SPIE* **9702**, 970210 (2016).
13. A. Darafsheh et al., "Fiber optic microprobes with rare-earth-based phosphor tips for proton beam characterization," *Proc. SPIE* **9700**, 97000Q (2016).
14. A. Darafsheh et al., "Separation of Čerenkov radiation in irradiated optical fibers by optical spectroscopy," *Proc. SPIE* **9315**, 93150Q (2015).
15. A. Darafsheh et al., "Phosphor-based fiber optic microprobes for ionizing beam radiation dosimetry," *Proc. SPIE* **9317**, 93170R (2015).
16. A. Darafsheh et al., "Characterization of rare-earth-doped nanophosphors for photodynamic therapy excited by clinical ionizing radiation beams," *Proc. SPIE* **9308**, 930812 (2015).
17. A. Darafsheh et al., "Phosphor-based fiber optic probes for proton beam characterization," *Med. Phys.* **42**(6), 3476–3476 (2015).
18. A. Darafsheh et al., "Optical characterization of novel terbium-doped nanophosphors excited by clinical electron and photon beams for potential use in molecular imaging or photodynamic therapy," *Med. Phys.* **41**(6), 436–436 (2014).
19. T. C. Zhu et al., "A flexible SiO₂ fiber detector array for proton beam range verification," *Med. Phys.* **44**(6), 2991 (2017).
20. A. Darafsheh et al., "Proton therapy dosimetry by using the scintillation of glass and plastic bare optical fibers," *Med. Phys.* **44**(6), 2858 (2017).
21. S. Beddar and L. Beaulieu, *Scintillation Dosimetry*, CRC Press, Boca Raton, Florida (2016).
22. S. Beddar, T. R. Mackie, and F. H. Attix, "Čerenkov light generated in optical fibres and other light pipes," *Phys. Med. Biol.* **37**(4), 925–935 (1992).
23. F. Therriault-Proulx et al., "On the nature of the light produced within PMMA optical light guides in scintillation fiber-optic dosimetry," *Phys. Med. Biol.* **58**(7), 2073–2084 (2013).
24. W. J. Yoo et al., "Development of a fiber-optic dosimeter based on modified direct measurement for real-time dosimetry during radiation diagnosis," *Meas. Sci. Technol.* **24**(9), 094022 (2013).
25. S. F. de Boer, A. S. Beddar, and J. A. Rawlinson, "Optical filtering and spectral measurements of radiation-induced light in plastic scintillation dosimetry," *Phys. Med. Biol.* **38**, 945–958 (1993).
26. M. A. Clift, P. N. Johnston, and D. V. Webb, "A temporal method of avoiding the Čerenkov radiation generated in organic scintillator dosimeters by pulsed mega-voltage electron and photon beams," *Phys. Med. Biol.* **47**, 1421–1433 (2002).
27. J. M. Fontbonne et al., "Scintillating fiber dosimeter for radiation therapy accelerator," *IEEE Trans. Nucl. Sci.* **49**(5), 2223–2227 (2002).
28. A. M. Frelin et al., "Spectral discrimination of Čerenkov radiation in scintillating dosimeters," *Med. Phys.* **32**(9), 3000–3006 (2005).
29. M. Guillot et al., "Spectral method for the correction of the Čerenkov light effect in plastic scintillation detectors: a comparison study of calibration procedures and validation in Čerenkov light-dominated situations," *Med. Phys.* **38**(4), 2140–2150 (2011).
30. J. A. Harrington, *Infrared Fibers and Their Applications*, SPIE Press, Bellingham, Washington (2004).
31. J. A. Harrington, "A review of IR transmitting, hollow waveguides," *Fiber Integr. Opt.* **19**(3), 211–227 (2000).
32. J. Lambert et al., "Čerenkov-free scintillation dosimetry in external beam radiotherapy with an air core light guide," *Phys. Med. Biol.* **53**(11), 3071–3080 (2008).
33. A. Darafsheh, "Optical super-resolution and periodical focusing effects by dielectric microspheres," PhD Dissertation, University of North Carolina, Charlotte (2013).
34. J. E. Melzer and J. A. Harrington, "Investigation of silver-only and silver/TOPAS® coated hollow glass waveguides for visible and NIR laser delivery," *Proc. SPIE* **9317**, 93170H (2015).
35. R. Robertson et al., "Optical imaging of Čerenkov light generation from positron-emitting radiotracers," *Phys. Med. Biol.* **54**, N355–N365 (2009).
36. R. S. Dothager et al., "Čerenkov radiation energy transfer (CRET) imaging: a novel method for optical imaging of PET isotopes in biological systems," *PLoS ONE* **5**(10), e13300 (2010).
37. M. A. Lewis et al., "On the potential for molecular imaging with Čerenkov luminescence," *Opt. Lett.* **35**(23), 3889–3891 (2010).
38. H. Liu et al., "Molecular optical imaging with radioactive probes," *PLoS ONE* **5**(3), e9470 (2010).
39. A. Ruggiero et al., "Čerenkov luminescence imaging of medical isotopes," *J. Nucl. Med.* **51**(7), 1123–1130 (2010).
40. A. E. Spinelli et al., "Čerenkov radiation allows in vivo optical imaging of positron emitting radiotracers," *Phys. Med. Biol.* **55**, 483–495 (2010).
41. G. Lucignani, "Čerenkov radioactive optical imaging: a promising new strategy," *Eur. J. Nucl. Med. Mol. Imaging* **38**(3), 592–595 (2011).
42. Y. Xu, H. Liu, and Z. Cheng, "Harnessing the power of radionuclides for optical imaging: Čerenkov luminescence imaging," *J. Nucl. Med.* **52**(12), 2009–2018 (2011).
43. D. L. Thorek et al., "Quantitative imaging of disease signatures through radioactive decay signal conversion," *Nat. Med.* **19**(10), 1345–1350 (2013).
44. V. Wood and N. L. Ackerman, "Čerenkov light production from the α -emitting decay chains of ²²³Ra, ²¹²Pb, and ¹⁴⁹Tb for Čerenkov luminescence imaging," *Appl. Radiat. Isot.* **118**, 354–360 (2016).
45. A. E. Spinelli et al., "Čerenkov and radioluminescence imaging of brain tumor specimens during neurosurgery," *J. Biomed. Opt.* **21**(5), 050502 (2016).
46. N. L. Ackerman, F. Boschi, and A. E. Spinelli, "Monte Carlo simulations support non-Čerenkov radioluminescence production in tissue," *J. Biomed. Opt.* **22**(8), 086002 (2017).
47. J. Axelsson et al., "Čerenkov emission induced by external beam radiation stimulates molecular fluorescence," *Med. Phys.* **38**(7), 4127–4132 (2011).
48. J. C. Finlay and A. Darafsheh, "Light sources, drugs, and dosimetry," Chapter 19 in *Biomedical Optics in Otorhinolaryngology: Head and Neck Surgery*, B. Wong and J. Ilgner, Eds., pp. 311–336, Springer, New York (2016).
49. B. Brichard et al., "Fibre-optic gamma-flux monitoring in a fission reactor by means of Čerenkov radiation," *Meas. Sci. Technol.* **18**(10), 3257–3262 (2007).
50. J. S. Cho et al., "Čerenkov radiation imaging as a method for quantitative measurements of beta particles in a microfluidic chip," *Phys. Med. Biol.* **54**(22), 6757–6771 (2009).
51. Z. W. Bell et al., "Measurement of neutron yields from UF₄," *IEEE Trans. Nucl. Sci.* **57**(4), 2239–2246 (2010).
52. W. J. Yoo et al., "Development of a Čerenkov radiation sensor to detect low-energy beta-particles," *Appl. Radiat. Isot.* **81**, 196–200 (2013).
53. K. W. Jang et al., "Feasibility of fiber-optic radiation sensor using Čerenkov effect for detecting thermal neutrons," *Opt. Express* **21**(12), 14573–14582 (2013).
54. A. K. Glaser et al., "Optical dosimetry of radiotherapy beams using Čerenkov radiation: the relationship between light emission and dose," *Phys. Med. Biol.* **59**(14), 3789–3811 (2014).
55. K. W. Jang et al., "Application of Čerenkov radiation generated in plastic optical fibers for therapeutic photon beam dosimetry," *J. Biomed. Opt.* **18**(2), 027001 (2013).
56. R. Zhang et al., "Oxygen tomography by Čerenkov-excited phosphorescence during external beam irradiation," *J. Biomed. Opt.* **18**(5), 050503 (2013).
57. A. K. Glaser et al., "Video-rate optical dosimetry and dynamic visualization of IMRT and VMAT treatment plans in water using Čerenkov radiation," *Med. Phys.* **41**(6), 062102 (2014).
58. A. Darafsheh et al., "The connection between Čerenkov light emission and radiation absorbed dose in proton irradiated phantoms," *Med. Phys.* **43**(6), 3418–3419 (2016).
59. J. V. Jelly, *Čerenkov Radiation and Its Applications*, Pergamon Press, London (1958).

60. P. R. Almond et al., "AAPM's TG-51 protocol for clinical reference dosimetry of high-energy photon and electron beams," *Med. Phys.* **26**(9), 1847–1870 (1999).

Arash Darafsheh is an assistant professor of radiation oncology in Washington University School of Medicine. He completed his postdoctoral fellowship, certificate in medical physics, and medical physics residency at the University of Pennsylvania. He has a PhD in optical science and engineering from UNC-Charlotte. His research interests are in the areas of optics and medical physics. He has pioneered immersed microsphere-assisted superresolution microscopy. He has published over 65 journal and conference papers, two book chapters, and a patent.

Jeffrey E. Melzer received his BS degree in materials science and engineering from Rutgers University, Piscataway, New Jersey, USA, in 2015. He is currently a PhD candidate in the College of Optical Sciences at the University of Arizona, Tucson, Arizona, USA, where his research focuses on optical manipulation and assembly via optical tweezers. His research interests include specialty fiber optics, metamaterials, and superresolution imaging.

James A. Harrington is a distinguished professor at Rutgers University. He has over 40 years of research experience in the area of optical properties of solids. Since 1977, he has worked on

all aspects of infrared fibers including fabrication, characterization, and applications. He is the inventor of the hollow sapphire and hollow glass waveguides, which are used today in certain laser surgical applications. His research is in the area of specialty fiber optics including passive hollow fibers for laser power delivery, fiber sensors, and active fibers centered on the fabrication of single-crystal fiber optics for use as fiber lasers.

Alireza Kassaee is a clinical associate professor in the Department of Radiation Oncology at the University of Pennsylvania. He completed his PhD at the State University of New York at Buffalo and completed his postdoctoral study in medical physics at the University of Chicago. His area of research focuses on characterization of clinical radiation beams including proton, photon, and electron beams using various radiation detectors. Recently, he has been studying characteristics and response of optical fibers for proton beam dosimetry.

Jarod C. Finlay is an assistant professor in the Department of Radiation Oncology at the University of Pennsylvania. He completed his PhD at the University of Rochester and postdoctoral study at the University of Pennsylvania in the areas of tissue optics and photodynamic therapy dosimetry. His work focuses on preclinical and clinical photodynamic therapy, and optical imaging for dosimetry in photodynamic and ionizing radiation therapies. He has published over 35 peer-reviewed papers and holds two patents.